Axisymmetric particle-element coupled method for deformation problems of geomaterial

AUTHOR(S):

Kiriyama, Takatoshi; Higo, Yosuke

CITATION:

Kiriyama, Takatoshi ...[et al]. Axisymmetric particle-element coupled method for deformation problems of geomaterial. Soils and Foundations 2022, 62(5): 101180.

ISSUE DATE:

2022-10

URL:

http://hdl.handle.net/2433/284577

HOSTED BY
ELSEVIER
Available online at www.sciencedirect.com
ScienceDirect
Soils and Foundations 62 (2022) 101180
www.elsevier.com/locate/sandf

Technical Note

Axisymmetric particle-element coupled method for deformation problems of geomaterial

Takatoshi Kiriyama [a,*], Yosuke Higo [b]

[a] *Center for Construction Engineering, Institute of Technology, Shimizu Corporation, 3-4-17, Etchujima, Koto-ku, Tokyo 135-8530, Japan*
[b] *Graduate School of Management (double appointment) Department of Urban Management, Graduate School of Engineering, C1-235 Kyotodaigaku-Katsura, Nishikyo-ku, Kyoto 615-8540, Japan*

Received 1 November 2021; received in revised form 29 April 2022; accepted 1 June 2022
Available online 3 August 2022

Abstract

Although grid-based particle methods are widely used for engineering deformation problems, due to their robustness in large deformation analyses, the computational cost of these methods is quite high compared with mesh-based methods. In 3D problems, the computational cost becomes even higher, whereas some mechanical systems can be regarded as axisymmetric, allowing them to be modeled as two-dimensional axisymmetric entities, resulting in a reduced computation cost. In order to decrease the computational cost further, arbitrary spatial discretization has been introduced to reduce the degrees of freedom in the system. The Particle-Element Coupled Method (PEM), the coupled method of the Material Point Method (MPM) and the Arbitrary Particle Domain Interpolation (APDI) method, enables a system to be discretized in arbitrary spatial resolutions. In this paper, PEM is extended to axisymmetric problems, whose formulation and applicability to geomaterial deformation are presented. Firstly, the axisymmetric MPM simulation of a granular column collapse experiment and its efficiency in computation are reported. Secondly, in the simulation of footing penetration, it is shown that the axisymmetric MPM and the axisymmetric PEM can be used to analyze large deformations that cannot be analyzed by mesh-based methods, such as the Finite Difference Method (FDM). The axisymmetric PEM yields equivalent average pressure–displacement relationships and shear strain distributions, realizing a reduction in the computation cost by half as much.

Keywords: Particle element coupled method; Material point method; Large deformation; Axisymmetric formulation

1. Introduction

The representative grid-based particle methods are Particle in Cell (PIC) (Harlow, 1956) in fluid mechanics and the Material Point Method (MPM) (Sulsky et al., 1994) in solid mechanics, both of which are in wide use due to their robustness in large deformation analyses. The characteristics of grid-based particle methods are: i) the physical space and calculation space are clearly separated; ii) interpolation functions link the physical and calculation spaces; and iii) interpolation functions have been defined from discrete (mass points) to continuum (elements).

While the methods have been used successfully for large deformation problems, the computational cost of the communication between the physical and calculation spaces is quite high compared with that of mesh-based analysis systems, such as the Finite Element Method, in which the physical and calculation spaces are identical. When subjecting three-dimensional (3D) problems to a grid-based particle

Peer review under responsibility of The Japanese Geotechnical Society.
* Corresponding author.
E-mail addresses: kiriyama@shimz.co.jp (T. Kiriyama), higo.yohsuke.5z@kyoto-u.ac.jp (Y. Higo).

https://doi.org/10.1016/j.sandf.2022.101180
0038-0806/

method, the computational cost becomes even higher, while some mechanical systems (e.g., vertical problems such as piles and circular tank/caisson installations) can be regarded as axisymmetric, allowing them to be modeled as two-dimensional axisymmetric entities from a geometrical viewpoint, resulting in a reduced computation cost.

In order to reduce the computational cost further, arbitrary spatial discretization has been introduced to decrease the proportional increase in the degrees of freedom (DOF) in the system when uniform discretization is used. One such spatial discretization system is the Particle-Element Coupled Method (PEM), proposed by Kiriyama and Higo (2020), that enables a system to be discretized in arbitrary spatial resolutions. PEM is a numerical technique that discretizes the target system in two domains. One domain is subjected to intensive large deformation discretized by particles, excluding mesh-tangling problems. The other domain is subjected to small deformation and is discretized by elements, resulting in arbitrary spatial discretization.

In their previous paper, Kiriyama and Higo (2020) demonstrated 2- and 3- dimensional examples using PEM. In the present paper, PEM is extended further to axisymmetric problems. Its formulation is presented, and the applicability of axisymmetric PEM to geomaterial deformation and its efficiency in computation are reported. In Section 2, the formulations of axisymmetric PEM are presented. In Section 3, the performance of axisymmetric MPM is reviewed and validated for deformation problems of geomaterials. In Section 4, axisymmetric PEM is applied to a large deformation problem.

2. Axisymmetric formulation of PEM

The Material Point Method (MPM) was initially proposed by Sulsky et al. (1994). The axisymmetric formulation of the method was also proposed by the same author (Sulsky and Schreyer, 1996). There was a problem in the calculation process of the original MPM, in which numerical oscillations were generated when material points crossed numerical grids. These oscillations were overcome by the introduction of the Generalized Interpolation Material Point (GIMP) method, in which the control domain of the material point is considered (Bardenhagen and Kober, 2004). An axisymmetric formulation of the GIMP method was proposed by Nairn and Guilkey (2014), and an application to pile penetration into a geomaterial has since been reported (Lorenzo et al., 2018). Convected Particle Domain Interpolation (CPDI) was proposed by Sadeghirad et al. (2013), in which a particle domain deforms arbitrarily considering the stretch and rotation of the particle domain in two dimensions, followed by Arbitrary Particle Domain Interpolation (APDI) proposed by Kiriyama and Higo (2020), in which 2- and 3-dimensional arbitrary particle domain interpolation functions are unified. Following the previous reports, the axisymmetric formulations of MPM and PEM in axisymmetric form are explained below.

2.1. Axisymmetric MPM

In this section, a short description of the axisymmetric formulation of MPM is given, following Sulsky and Schreyer (1996). A cylindrical coordinate system is considered with coordinates (r, θ, z) and z along the symmetry axis.

The momentum equation is described as.

$$\rho \dot{\boldsymbol{v}} = \nabla \cdot \boldsymbol{\sigma} + \rho \boldsymbol{b} \tag{1}$$

where ρ, $\boldsymbol{v}$, $\boldsymbol{\sigma}$, and $\boldsymbol{b}$ are the density, velocity, Cauchy stress tensor, and specific body force, respectively. Multiplying by a test function, and using the divergence theorem, the weak form of the momentum equation is described as.

$$\int_{\Omega} \rho \boldsymbol{w} \cdot \dot{\boldsymbol{v}} dA = -\int_{\Omega} \rho \boldsymbol{\sigma}^s : \nabla \boldsymbol{w} dA + \int_{\partial\Omega} \boldsymbol{w} \cdot \boldsymbol{\tau} ds + \int_{\Omega} \rho \boldsymbol{w} \cdot \boldsymbol{b} dA \tag{2}$$

where $\boldsymbol{w}$, A, and $\boldsymbol{\tau}$ are the test function, a discretized element of area $\Omega(A = r \cdot dr \cdot dz)$, and the prescribed traction, respectively. The weak form of the governing equation is discretized by the MPM numerical process using the following interpolation functions:

$$\sum_{i=1}^{N_n} \boldsymbol{w}_i(t) \cdot \sum_{j=1}^{N_n} m_{ij}(t) \dot{\boldsymbol{v}}(t) = -\sum_{i=1}^{N_n} \sum_{p=1}^{N_p} m_p \boldsymbol{\sigma}^s\left(x_p(t), t\right) : (\boldsymbol{w}_i(t)) \nabla S_{ip} + \sum_{i=1}^{N_n} \boldsymbol{w}_i(t) \cdot \boldsymbol{\tau}(t) + \sum_{i=1}^{N_n} \boldsymbol{w}_i(t) \cdot \boldsymbol{b}_i(t) \tag{3}$$

where N_n, m_{ij}, N_p, and m_p are the number and mass matrices of the spatial nodes and material points, respectively, and $\boldsymbol{\sigma}^s$ and $\boldsymbol{\tau}$ are the specific stress $(\boldsymbol{\sigma} = \rho \boldsymbol{\sigma}^s)$ and the discrete applied traction, respectively. x_p is the material point coordinate. S_{ip} and ∇S_{ip} are the nodal base functions associated with node (i) at the material point (p) and its gradient, respectively.

The first term on the right-hand side of Eq. (3) can be written in terms of the internal force as.

$$-\sum_{i=1}^{N_n} \sum_{p=1}^{N_p} m_p \boldsymbol{\sigma}^s\left(x_p(t), t\right) : (\boldsymbol{w}_i(t)) \nabla S_{ip} = \sum_{i=1}^{N_n} \boldsymbol{w}_i(t) \cdot f_i^{int} \tag{4}$$

Especially with axisymmetric cylindrical coordinates, the components of the internal force are $f_i^{int} = \left\{ f_{r,i}^{int}, f_{z,i}^{int} \right\}$, where.

$$f_{r,i}^{int} = -\sum_{p=1}^{N_p} \frac{m_p}{\rho_p} \left\{ \sigma_{rr,p} \frac{\partial S_{ip}}{\partial r} + \sigma_{rz,p} \frac{\partial S_{ip}}{\partial z} + \sigma_{\theta\theta,p} \frac{S_{ip}}{r_p} \right\} \tag{5}$$

$$f_{z,i}^{int} = -\sum_{p=1}^{N_p} \frac{m_p}{\rho_p} \left\{ \sigma_{rz,p} \frac{\partial S_{ip}}{\partial r} + \sigma_{zz,p} \frac{\partial S_{ip}}{\partial z} \right\} \tag{6}$$

The numerical procedure after the discretization of the governing equation is performed by the update stress first method (USF) (Sulsky et al., 1994), update stress last method (USL) (Bardenhagen, 2002), or update stress average method (USAVG) (Nairn, 2003), etc. In the following

simulations, USAVG is implemented in explicit form along with the Euler time integration as the numerical procedure for MPM.

2.2. Axisymmetric PEM

Regarding the deformation characteristics of geomaterials, deformation tends to concentrate in a specific area where shear strain localization occurs, and intensive large deformation can be expected in this region. In order to simulate this localized shear deformation, a fine spatial discretization of the material points is necessary. However, providing sufficient material points to simulate localization causes an excessive increase in the computational cost even with an axisymmetric calculation. While localization tends to occur in a specific area, relatively smaller deformation can be expected in other areas. Therefore, it is computationally efficient to define a fine spatial discretization only in the area where large deformation is expected, with a coarse arrangement in other areas. Following this idea, Kiriyama and Higo (2020) proposed the mixed use of different interpolation functions in different areas, which enables the discretization of the system with varying spatial resolutions. This method is called the Particle-Element Coupled Method (PEM). It entails arranging the material points with a uGIMP or cpGIMP interpolation function in the area where large deformation is expected, while the material points with a CPDI or APDI interpolation function are arranged elsewhere. Here, uGIMP stands for the unchanged/uniform GIMP interpolation, in which the control domain is constant throughout the whole process, while cpGIMP stands for contiguous particle GIMP interpolation, in which the control domain is updated during the simulation (Bardenhagen and Kober, 2004). The u/cpGIMP interpolation method does not fully consider the stretching or rotation of the material points, meaning it has more of a 'particle' characteristic than an element characteristic. Both CPDI and APDI, considering stretching and rotation, treat material points as 'elements'.

The formulation of PEM is described in the following. The system is assumed to be divided into two subdomains: one is the primary deformable domain in which large deformation is expected; the other is the subsidiary deformable domain in which smaller deformation is expected. The governing equation is divided into the following two equations with a continuity condition along the common boundary:

$$\int_{\Omega_1} \rho \boldsymbol{w}_1 \cdot \dot{\boldsymbol{v}} d\Omega_1 = -\int_{\Omega_1} \rho \boldsymbol{\sigma}^s : \nabla \boldsymbol{w}_1 d\Omega_1 + \int_{\partial\Omega_1} \boldsymbol{w}_1 \cdot \boldsymbol{\tau} dS_1 + \int_{\Omega_1} \rho \boldsymbol{w}_1 \cdot \boldsymbol{b} d\Omega_1 \quad (7)$$

$$\int_{\Omega_2} \rho \boldsymbol{w}_2 \cdot \dot{\boldsymbol{v}} d\Omega_2 = -\int_{\Omega_2} \rho \boldsymbol{\sigma}^s : \nabla \boldsymbol{w}_2 d\Omega_2 + \int_{\partial\Omega_2} \boldsymbol{w}_2 \cdot \boldsymbol{\tau} dS_2 + \int_{\Omega_2} \rho \boldsymbol{w}_2 \cdot \boldsymbol{b} d\Omega_2 \quad (8)$$

where $\boldsymbol{w}_1$ and $\boldsymbol{w}_2$ are the test functions for the independent divided domains. The spatial continuity condition along their common boundary is described as.

$$u_{v,1} = u_{v,2} \quad on \quad \partial\Omega_1 \cap \partial\Omega_2 \quad (9)$$

where u_v is the displacement at a vertex of each discretized domain. The interaction terms are included in Eqs. (7) and (8) in the original paper, while the interaction terms are cancelled out after the discretization and gathering of the grid force at the grid point, as long as the same spatial discretization is maintained along the boundary. Eq. (9) is the condition for the cancellation of the interaction terms, which requires the same spatial resolution along the common boundary. This means that the particles/elements with control domains of the same size are arranged side by side along the boundary; otherwise, holey-particle problems occur (Brannon, 2014).

The two independent governing equations, Eqs. (7) and (8), are discretized independently, so that different interpolation functions can be applied. This means that the different parts of the system use different interpolation functions independently, realizing the mixed use of different interpolation functions. This methodology is applicable even in 2D, axisymmetric, and 3D coordinate systems. While any combination of them is applicable in the above numerical process, it is noted that the spatial continuity should be satisfied by discretizing the boundary elements of both domains at the same spatial resolution.

3. Performance of axisymmetric MPM

Prior to the application of the axisymmetric PEM to deformation problems, it is necessary to understand the performance of the existing interpolation functions in axisymmetric form. Various interpolation functions have been proposed for grid-based particle methods (Sulsky et al., 1994; Bardenhagen and Kober, 2004; Sadeghirad et al., 2013; Kiriyama and Higo, 2020). In axisymmetric formulations, these interpolation functions are implemented in the manner described in Section 2. In order to understand the performance of each interpolation function in axisymmetric form, the following sand column collapse experiments are simulated.

3.1. Granular column collapse simulation

The experiment used for validation is comprised of a series of observations of a granular column collapse by Lajeunesse (2004), in which granular columns (of glass beads), with various aspect ratios, are formed in an acrylic cylinder. By instantaneously removing the cylinder, the columns are subjected to free horizontal spreading. In the experiment, snapshots of the granular column collapse and deposition are obtained using a high-speed digital camera focused on the sides of the columns.

Of the various experimental aspect ratios, columns with initial aspect ratios of 0.56, 0.8, and 5.4 are simulated by

axisymmetric MPM, in which the cpGIMP interpolation function is used. The analysis cases and conditions are described in Fig. 1, and the material properties are listed in Table 1. The columns are modeled as axisymmetric cylinders with the axisymmetric axis located along the left boundary of the numerical grids. The constitutive model for the geomaterials is implemented using an elasto-plastic formulation with the Mohr-Coulomb criterion for both yield and potential functions. Young's modulus (E) and the internal frictional angle (ϕ), given in Table 1, are determined by carrying out a sensitivity analysis for Case 1 beforehand. The dilatancy angle (ψ) is set to be constant at zero because the simulated granular material shows no plastic volumetric change at high strain. The columns are subjected to gravitational force and, after reaching initial equilibrium, the fixed condition along the column sides is removed, allowing the columns to spread horizontally.

Fig. 2 compares the experimental results (Lajeunesse, 2004) with the numerical simulations for the three aspect ratios, with the outlines of the granular column collapse shown by solid lines at time intervals of 0.02 s. The horizontal and vertical axes in the figure are normalized by dividing the radial coordinate (r) and height (h), respectively, by the initial column radius (R_i). These results demonstrate that the numerical method can well simulate the experimental observations throughout the process of

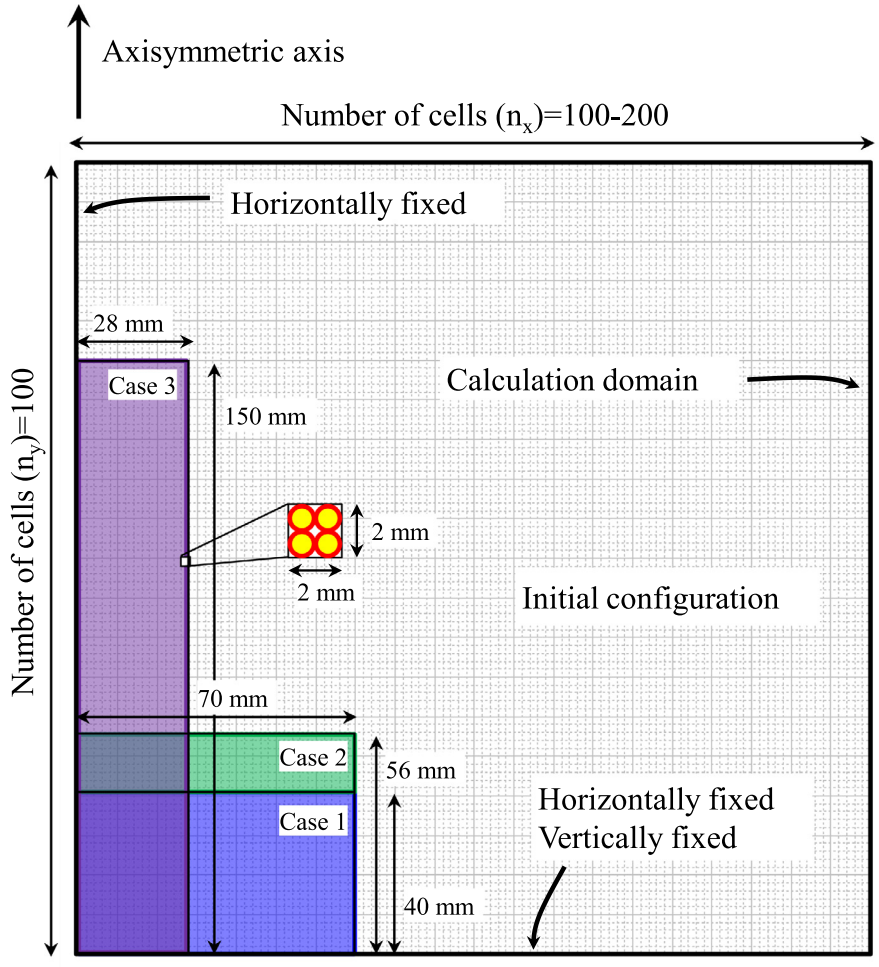

Fig. 1. Initial configuration and numerical conditions of granular column collapse.

Table 1
Numerical conditions and material properties of granular column collapse.

Material No.	Radius R m	Height H m	Aspect ratio a –	Young's modulus E kPa	Poisson's ratio v –	Unit weight γ kN/m^3	Internal frictional angle ϕ deg.	Cohesion c kPa
1	0.0705	0.03948	0.56	100	0.333	15.10	25	0.0
2	0.0705	0.05640	0.80	100	0.333	16.14	25	0.0
3	0.0280	0.15120	5.40	100	0.333	15.79	25	0.0

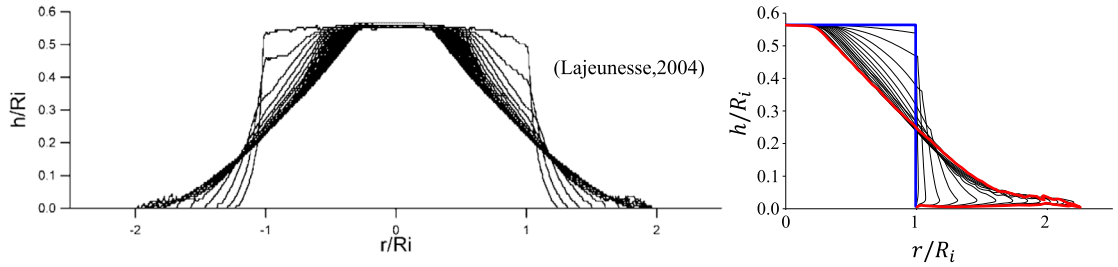

(i) Observed (ii) Simulation

(a) Case 1: aspect ratio a=0.56

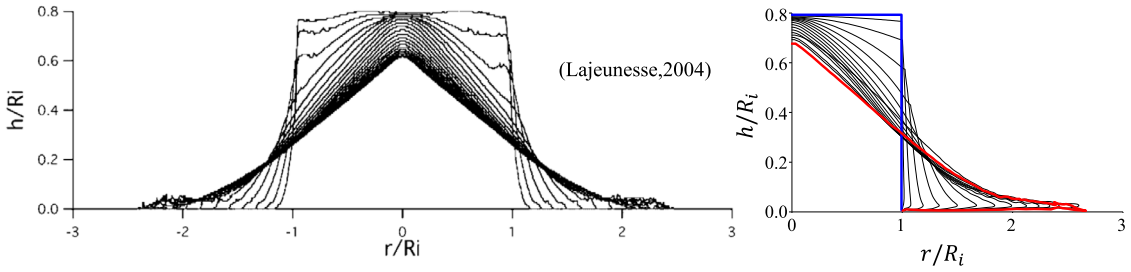

(i) Observed (ii) Simulation

(b) Case 2: aspect ratio a=0.8

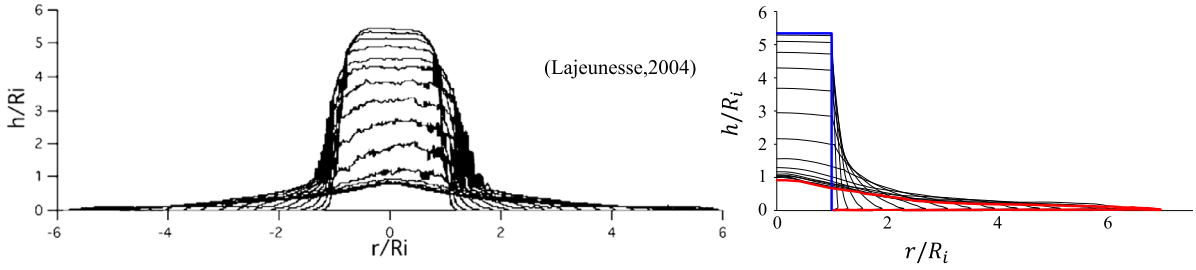

(i) Observed (ii) Simulation

(c) Case 3: aspect ratio a=5.4

Fig. 2. Outlines of column collapse. Numerical simulations by axisymmetric MPM(cpGIMP) results are compared with snapshots of sand column collapse (Lajeunesse, 2004). Time interval is 0.02(s). Blue and red lines correspond to the initial and final deposition outlines, respectively, of the column. * (i) is originally in Lajeunesse, 2004, and edited for comparison. (For interpretation of the references to colour in this figure legend, the reader is referred to the web version of this article.)

the granular column collapse. Focusing on the residual height (H_f) and horizontal spread ($R_f - R_i$), the simulation results are compared with the empirical equations for the column collapse in Fig. 3. Here, both axes are normalized by the initial radius (R_i). The empirical equations are those reported by Lajeunesse et al. (2006) and Lube et al. (2004) as follows:

Lajeunesse et al. (2006)

$$\frac{H_f}{R_i} = \begin{cases} a & a \le \lambda_1 \\ \lambda_1 & a > \lambda_1 \end{cases} \tag{10}$$

$$\frac{R_f - R_i}{R_i} = \begin{cases} \lambda_2 a & a \le \lambda_4 \\ \lambda_3 a^{1/2} & a > \lambda_4 \end{cases} \tag{11}$$

Lube et al. (2004)

$$\frac{H_f}{R_i} = \begin{cases} a & a \le 0.86 \\ 0.88a^{1/6} & a > 0.86 \end{cases} \tag{12}$$

$$\frac{R_f - R_i}{R_i} = \begin{cases} 1.24a & a \le 1.7 \\ 1.6a^{1/2} & a > 1.7 \end{cases} \tag{13}$$

λ_1–λ_4 are set here as ($\lambda_1 = 0.7$, $\lambda_2 = 1.24$, $\lambda_3 = 1.8$, $\lambda_4 = 2.11$) by the present authors.

According to Fig. 3, the simulation shows a good agreement with the empirical equations in terms of the residual height (H_f), while it overestimates the horizontal spread ($R_f - R_i$). This overestimation may result from the use of the continua theory in the numerical method, which is not consistent with the material behavior near the furthest collapse front, where the granules behave discretely around the axisymmetric axis.

3.2. Comparison of axisymmetric and 3D simulations

The axisymmetric formulation has advantages in that the DOF and computation requirements are fewer than those for the 3D analysis. In order to understand how efficient the axisymmetric formulation is, in terms of the DOF and computation time, the numerical results obtained by both the axisymmetric and 3D MPM(cpGIMP) simulations are compared. The target system is the same as that of the set of experiments by Lajeunesse (2004) simulated in the previous section. In the 3D analysis, the granular columns are simulated as quarter models with the same spatial resolution as the axisymmetric model and using the same material properties given in Table 1.

Fig. 4 shows the total displacements at (i) 0.04 s, (ii) 0.10 s, (iii) 0.16 s, and (iv) the final deposition, respectively. According to this figure, the material behaves continuously in both the axisymmetric and 3D MPM(cpGIMP) simulations until 0.16 s. At the final deposition, the material remains continuous throughout the deposition in the axisymmetric case, while it is deposited discretely in 3D around the collapse front. The displacements in Fig. 4 are consistent until 0.16 s, while at the final deposition, the 3D simulation granules deposit at a greater distance than the axisymmetric simulation granules. This discrepancy arises from the differing assumptions about the material behavior around the axisymmetric axis: either continuous or discrete. That is, the axisymmetric formulation assumes continuous behavior, while the 3D formulation assumes discrete behavior. Thus, for problems involving discrete behavior around the axisymmetric axis, it is necessary to use a 3D model, while an axisymmetric analysis is still applicable if it is acceptable to assume continuous behavior even around the axisymmetric axis.

Table 2 compares the computational requirements for running these axisymmetric and 3D models. The number of particles modeled in the axisymmetric model is one order less than that in the 3D model, and the computation time is two orders less. This shows the clear reduction in computational and modeling costs when using the axisymmetric model.

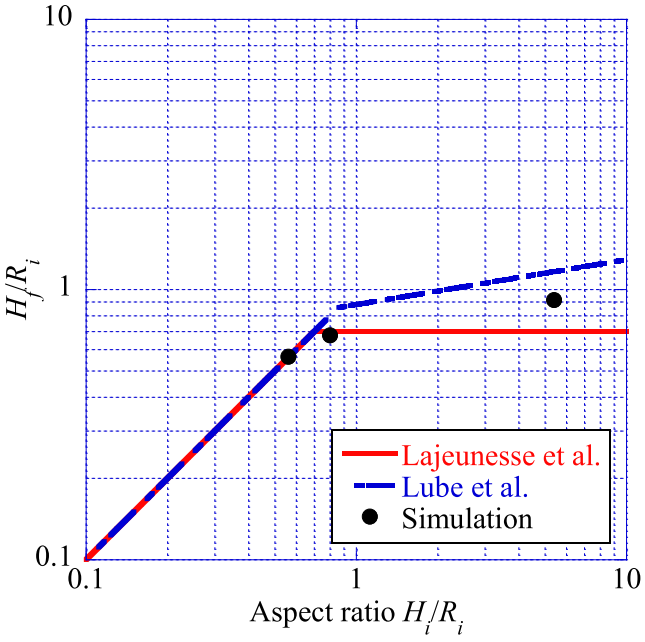

(a) Residual height

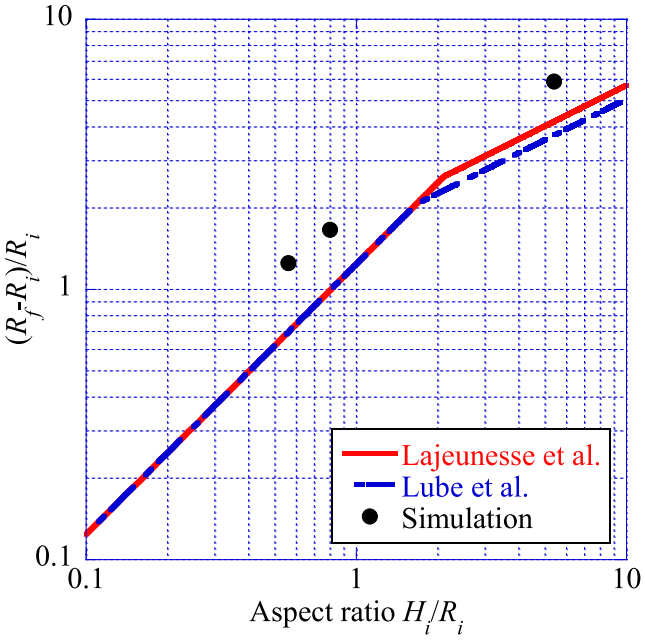

(b) Horizontal spread

Fig. 3. Comparison between axisymmetric MPM (cpGIMP) and empirical equation.

4. Applicability of axisymmetric PEM

The applicability of the axisymmetric formulation of the PEM to deformation problems of geomaterials is discussed in this section, focusing on the footing penetration problem. Firstly, the axisymmetric MPM(GIMP) and the Finite

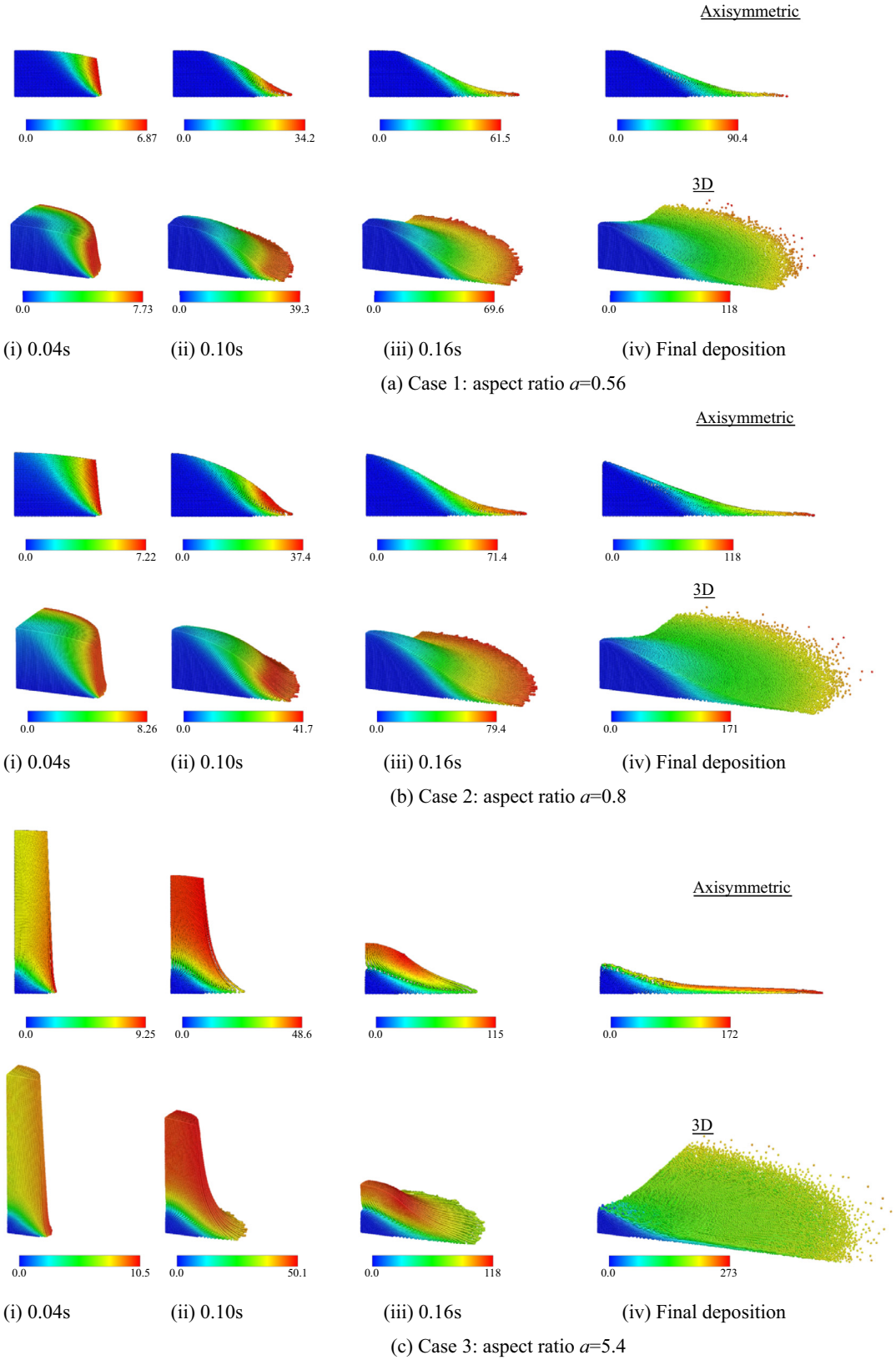

Fig. 4. Total displacement contours by axisymmetric and 3D MPM(cpGIMP) during collapse of sand columns (unit: mm).

Difference Method (FDM) (ITASCA, 2018) are compared under large deformation, followed by the PEM simulation in which there is a discussion on how the combination of particles and elements affects the numerical results.

Table 2
Comparison of computations between axisymmetric and 3D models.

	Modelling	Number of entities		Computation
		Particle	Grid	min./hour
Case 1	2D axis.	2,802	20,000	16 min.
	3D (a quarter model)	1,53,320	40,00,000	47 h
Case 2	2D axis.	3,922	20,000	21 min.
	3D (a quarter model)	2,14,648	40,00,000	75 h
Case 3	2D axis.	4,202	20,000	23 min.
	3D (a quarter model)	91,200	80,00,000	45 h

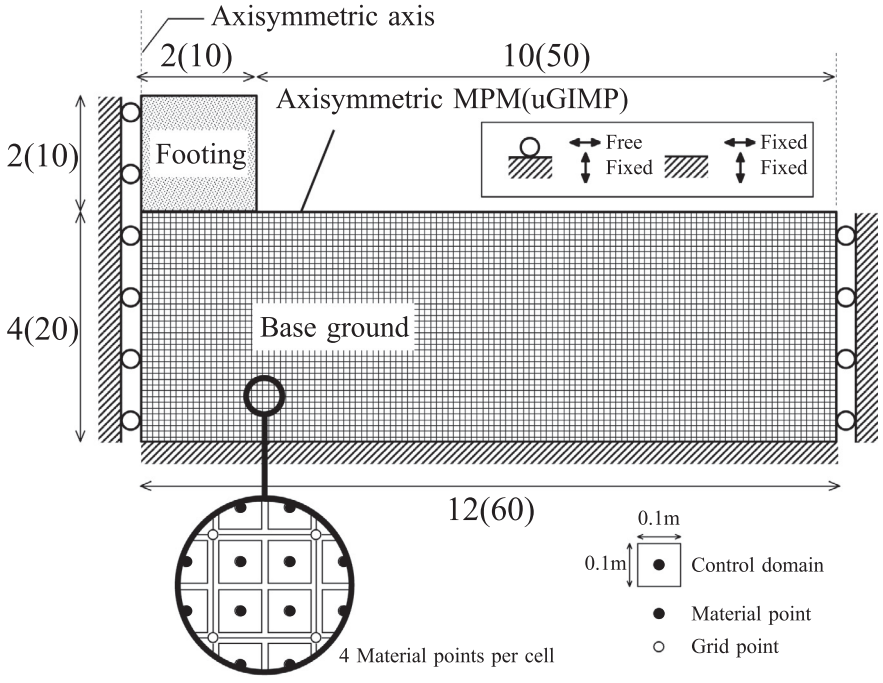

(a) Particle model plotted by particle control domain

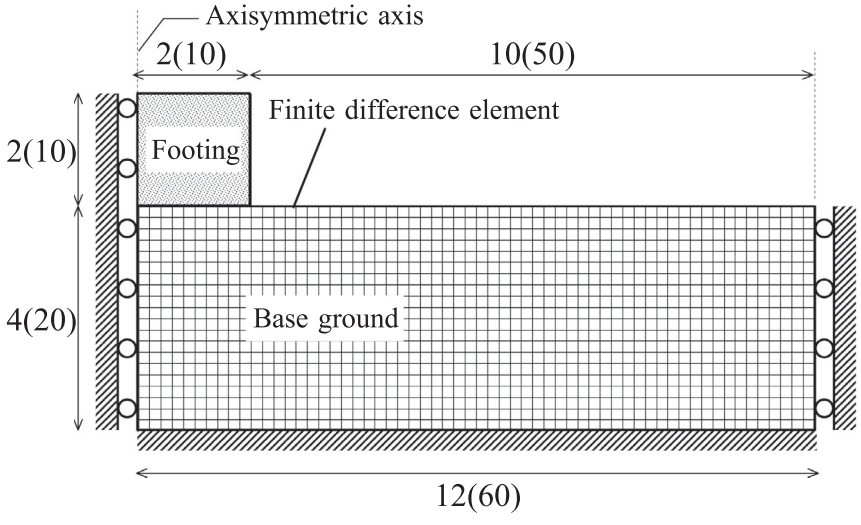

(b) Finite difference model plotted by element connectivity

Fig. 5. Spatial discretizations in axisymmetric MPM(uGIMP) and FDM for footing penetration into base ground. The numbers show the length in meters, followed by the number of grids (in axisymmetric MPM) or elements (in FDM) (unit:m).

Table 3
Material properties of footing penetration problem.

	Young's modulus E kPa	Poisson's ratio v –	Unit weight γ kN/m^3	Internal frictional angle ϕ deg.	Cohesion c kPa	Dilatancy angle ψ deg.
Footing	200,000	0.3	50 to 1500	–	–	–
soil	20,000	0.3	15	20	50	0/20

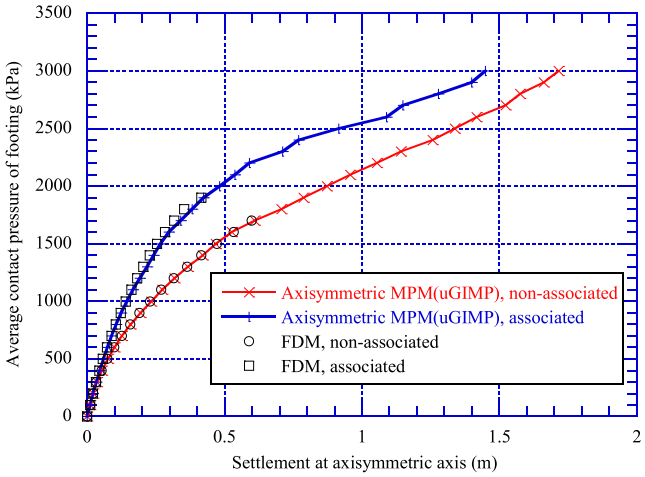

Fig. 6. Average pressure–displacement relationships by axisymmetric MPM(uGIMP) and FDM under non-associated/associated flow.

4.1. Behavior of geomaterials beneath footings under large deformation

Footing penetration is one of the classical deformation problems of geomaterials. As explained in the literature (Zienkiewicz et al., 1975; Chen and Mizuno, 1990; Bui et al., 2008; Kiriyama and Higo, 2020), the footings and base grounds of similar systems are prepared to allow for a comparison of GIMP and FDM. Fig. 5 shows the numerical models used for GIMP and FDM. The system is modeled as axisymmetric with the axisymmetric axis on the left side. The numbers in this figure indicate the length of each part, followed by the number of grids/elements in the GIMP/FDM. Fig. 5(a) is drawn by particle arrangement, behind which a numerical grid is arranged regularly with the same spatial resolution as FDM. The material properties are listed in Table 3. Both non-associated and

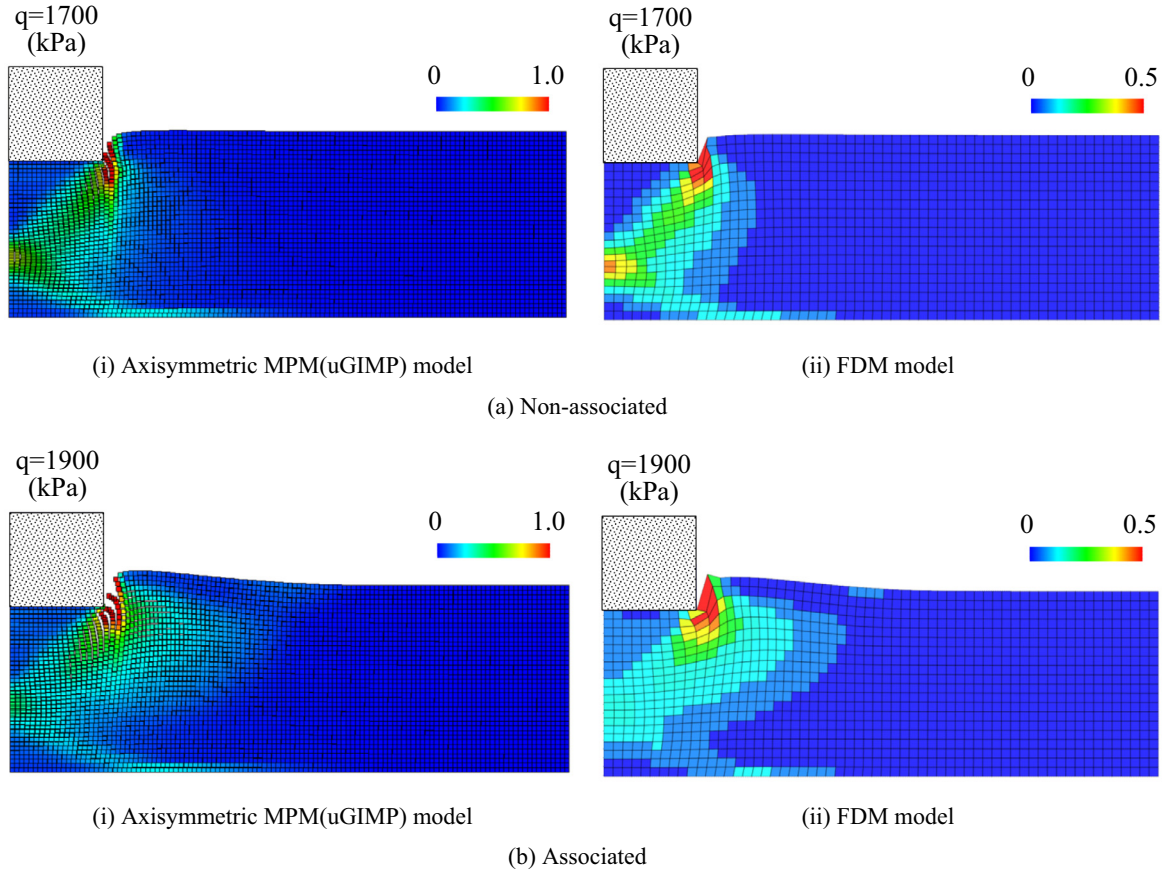

Fig. 7. Comparison of maximum shear strain distributions between axisymmetric MPM(uGIMP) and FDM models with non-associated/associated flow.

associated flow conditions are employed to understand how plastic volumetric change affects the geomaterial behavior. Here, 'non-associated' means that the dilatancy angle in the potential function is set to be constant at zero, assuming the material shows no positive/negative plastic volumetric strain, while 'associated' means that the dilatancy angle in the potential function is set to be the same as the internal frictional angle. The system is subjected to a gravitational force of 1g, while the density of the footing is changed incrementally after the system reaches equilibrium under each external force level.

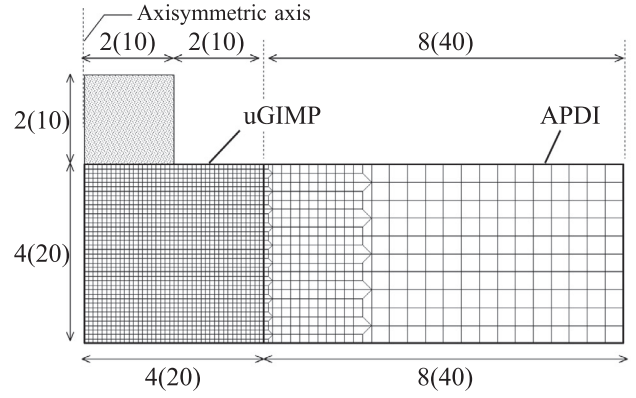

(a) Model-1

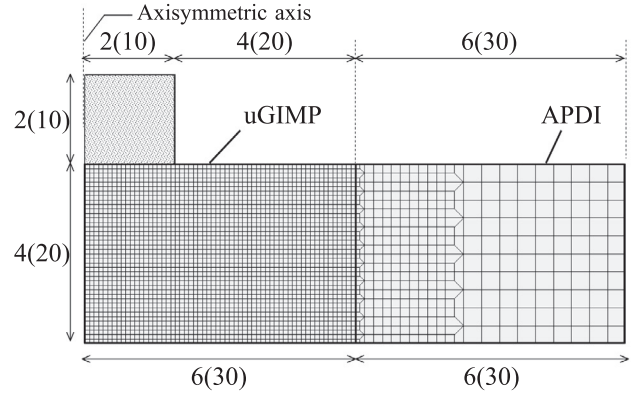

(b) Model-2

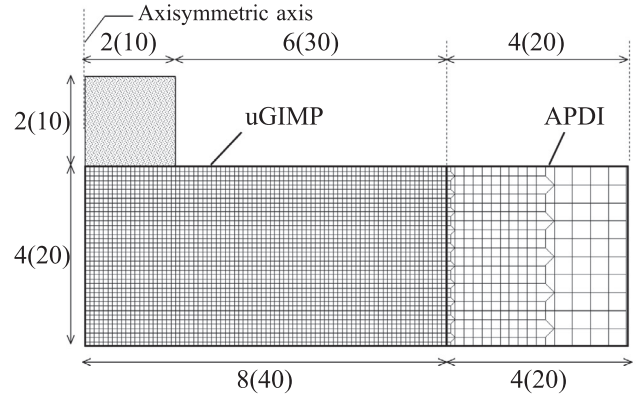

(c) Model-3

Fig. 8. PEM models for footing penetration into base ground (unit:m).

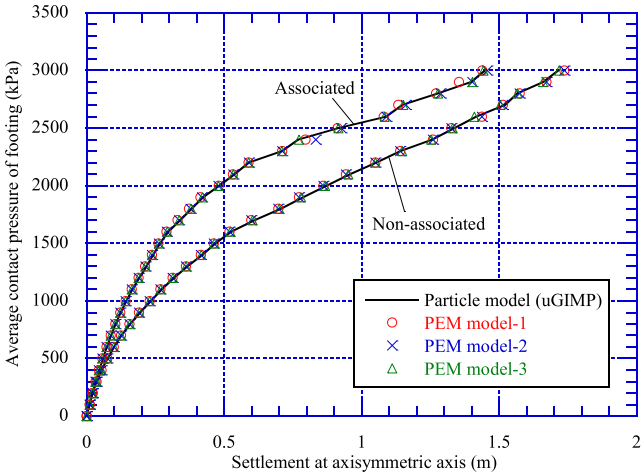

Fig. 9. Comparison of average pressure–displacement curves among Particle (uGIMP) and PEM models under non-associated/associated flow.

Fig. 6 shows the average pressure–displacement relationships by uGIMP and FDM. The results agree well under non-associated and associated flow conditions. The vertical axis in the figure is the average contact pressure under the footing, which is calculated by dividing the total self-weight of the footing by the contact area. The settlement given by uGIMP in Fig. 6 is monitored at a material point immediately beneath the footing nearest the axisymmetric axis, while the settlement given by FDM is monitored at a grid-point immediately beneath the footing along the axisymmetric axis. The discrepancy arises from the differing numerical methods, implementation, monitoring positions, and so on. According to Fig. 6, FDM simulated the system over a limited range until 1700 kPa in the non-associated flow and until 1900 kPa in the associated flow. Thereafter, geometrical errors occurred after the contact pressure level increased further. Fig. 7 shows the maximum shear strain distributions for both uGIMP and FDM, in which the particles in uGIMP and the elements in FDM are colored, respectively. The contour range is adjusted so that the shear strain colors of the particles and the elements are equivalent to each other. This shows that uGIMP and FDM are in good agreement with each other under both non-associated and associated flow conditions. It is noticeable that uGIMP is able to simulate

Table 4
Summary of simulations and their computational costs.

	Number of entities			Computation time (h)
	Footing	Base ground		
	Particle	Particle	Element	
GIMP model	400	4,800	0	36.5
PEM model-1	400	1600	410	19
PEM model-2	400	2400	360	23
PEM model-3	400	3200	310	28

the system until the final loading condition of 3000 kPa in this series, while FDM is not, meaning that the grid-based particle method has advantages over the mesh-based method because it is free from geometrical errors and is able to continue the numerical process with more robustness.

4.2. Comparison of particle (uGIMP) model and PEM models

It is worth noting that, in the particle-based method, when the deformation is large, a significant part of the domain remains in the regime of small deformation even

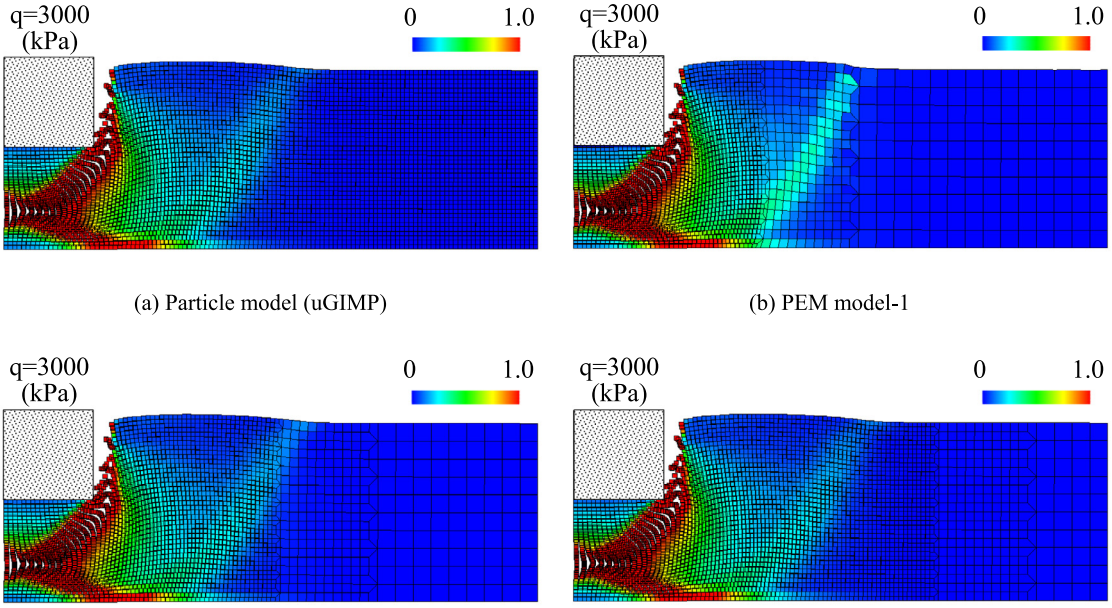

(a) Particle model (uGIMP) (b) PEM model-1

(c) PEM model-2 (d) PEM model-3

Fig. 10. Comparison of maximum shear strain distributions at 3000 kPa under non-associated flow.

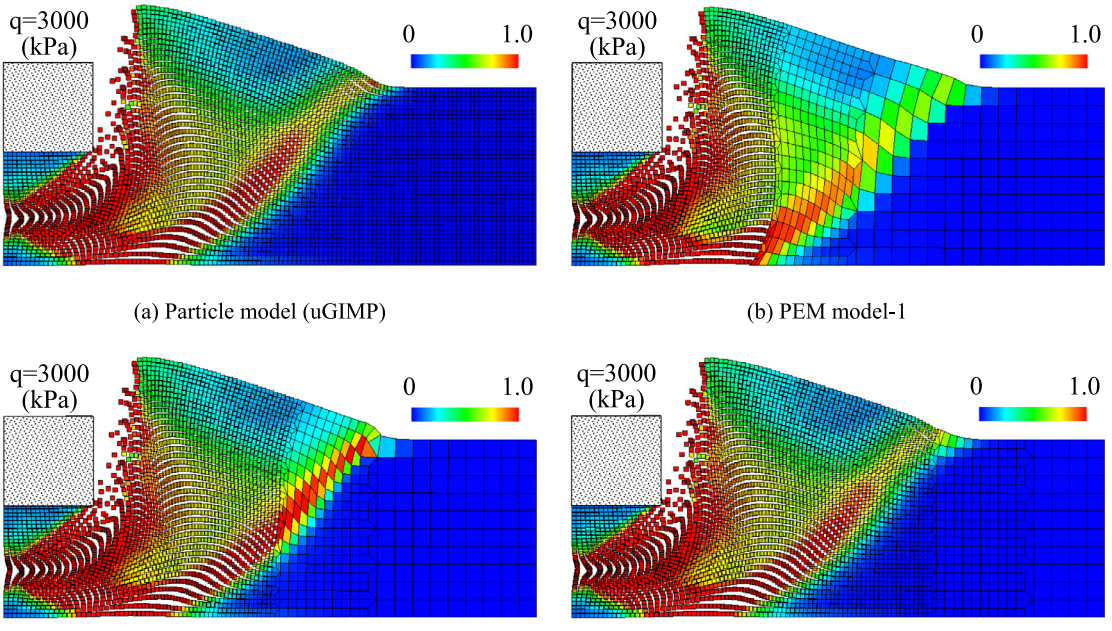

(a) Particle model (uGIMP) (b) PEM model-1

(c) PEM model-2 (d) PEM model-3

Fig. 11. Comparison of maximum shear strain distributions at 3000 kPa under associated flow.

though the whole domain is modeled by particles. In order to reduce the number of particles in the domain where the particles undergo small deformation, PEM is further extended to the axisymmetric system according to the axisymmetric formulation in Section 2.

In order to understand the effectiveness and efficiency of the axisymmetric PEM, three PEM models are prepared, as described in Fig. 8, in which particles are arranged from the center of the footing to one, two, and three times the footing radius away from the side of the footing, with other areas being modeled as elements. The boundary and load conditions, and the material properties applied to this model, are the same as those described in Fig. 5 and in Table 3.

Fig. 9 shows the resulting average pressure–displacement relationships. Under both non-associated and associated conditions, the average pressure–displacement results are comparable. Thus, for footing penetration problems, any of the PEM models is effective compared with the particle model (uGIMP in Fig. 6). As shown in Table 4, PEM model-1 can save close to half the computational effort compared with the particle model. That is, from the viewpoint of the computational cost (memory and time), PEM model-1 may be said to be the most computationally efficient. The difference among the three models is dependent on the spatial resolution and deformation ability of the geometry. Figs. 10 and 11 illustrate the maximum shear strain distributions. In the case of the non-associated flow (Fig. 10), an increase in shear strain is seen up to less than twice the footing radius away from the footing side, while in the case of the associated flow (Fig. 11), the range in increased shear strain extends to more than three times the radius. Under the associated flow, the geomaterial exhibits positive dilation as it deforms in shear. In the footing penetration system, that positive dilation generates additional lateral pressure, inducing the larger area of the base ground subjected to passive earth pressure.

5. Conclusions

The aim of this work was to extend the Particle-Element Coupled Method (PEM) to axisymmetric problems. The axisymmetric grid-based particle method was validated by a comparison with the experimental results for a granular column collapse. The simulation showed a good agreement with the experimental results in terms of the process of the granular column collapse, residual height, and horizontal spread. This means that the method is applicable as long as the geomaterials do not exhibit any discrete behavior in the circular direction.

The axisymmetric grid-based particle method was compared with the mesh-based method (FDM), where it was shown to provide a solution that is comparable with that of FDM, but it also provided a robust solution under large deformation, where the FDM numerical process cannot proceed. The method was then extended further to the Particle-Element Coupled Method in an axisymmetric form, demonstrating its applicability to geomaterials and its efficiency in terms of the computational cost. The axisymmetric PEM was shown to yield equivalent average pressure–displacement relationships and shear strain distributions to the axisymmetric particle method, realizing a reduction in computation cost by half as much.

References

Bardenhagen, S.G., 2002. Energy conservation error in the material point method for solid mechanics. J. Comput. Phys. 180, 383–403.
Zienkiewicz, O.C., Humpheson, C., Leweis, R.W., 1975. Associated and non-associated visco-plasticity and plasticity in soil mechanics. Geotechnique 25 (4), 671–689.
Brannon, R.M., 2014. Holey Particle Basis functions for 2D CPDI, University of Utah, Computational Solid Mechanics Group (accessed 2022 April 6th). https://csmbrannon.net/2014/03/09/holey-particle-basis-functions-for-2d-cpdi/.
Bardenhagen, S.G., Kober, E.M., 2004. The generalized interpolation material point method. Computer Modeling in Engineering and Science 5 (6), 477–495. https://doi.org/10.3970/cmes.2004.005.477, In press.
Bui, H.H., Fukagawa, R., Sako, K., Ohno, S., 2008. Lagrangian meshfree particles method (SPH) for large deformation and failure flows of geomaterial using elastic-plastic soil constitutive model. Int. J. Numer. Anal. Meth. Geomech. 32 (12), 1537–1570.
Chen, W.F., Mizuno, E., 1990. Nonlinear Analysis in Soil Mechanics: Theory and Implementation. Elsevier, Amsterdam.
Harlow, F.H., 1956. A Machine Calculation Method for Hydrodynamic Problems. Los Alamos Scientific Laboratory report LAMS.
ITASCA consulting group, 2018. FLAC3D version 5.0 manuals; theory and backgrounds.
Kiriyama, T., Higo, Y., 2020. Arbitrary particle domain interpolation method and application to problems of geomaterial deformation. Soils and Foundations 60 (6), 1422–1439.
Lajeunesse, E., 2004. Spreading of a granular mass on a horizontal plane. Phys. Fluids 16 (7).
Lajeunesse, E., Quantin, C., Allemand, A., Delacourt, C., 2006. New insights on the runout of large landslides in the Valles-Marineris canyons, Mars. Geophys. Res. Lett. 33, L04403.
Lorenzo, R., da Cunha, R.P., Cordao, M.P., Nairn, J.A., 2018. Numerical simulation of installation of jacked piles in sand using material point method. Can. Geotech. J. 55, 131–146.
Lube, G., Huppert, H.E., Sparks, R.S.J., Hallworth, M.A., 2004. Axisymmetric collapses of granular columns. J. Fluid Mech. 508, 175–199.
Nairn, J.A., 2003. Material point method calculations with explicit cracks. Comput. Model. Eng. Sci. 4 (6), 649–663.
Nairn, J.A., Guilkey, J.E., 2014. Axisymmetric form of the generalized interpolation material point method. Int. J. Numer. Meth. Eng. 101 (2), 127–147.
Sadeghirad, A., Brannon, R.M., Guilkey, J.E., 2013. Second-order convected particle domain interpolation (CPDI2) with enrichment for weak discontinuities at material interfaces. Int. J. Numer. Meth. Eng. 95 (12), 928–952.
Sulsky, D., Chen, Z., Schreyer, H.L., 1994. A particle method for history-dependent materials. Comput. Methods Appl. Mech. Eng. 118, 179–196.
Sulsky, D., Schreyer, H.L., 1996. Axisymmetric form of the material point method with applications to upsetting and Taylor impact problems. Comput. Methods Appl. Mech. Eng. 139, 409–429.